Journal of Biomechanics 41 (2008) 3496–3501

Contents lists available at ScienceDirect

Journal of Biomechanics

journal homepage: www.elsevier.com/locate/jbiomech
www.JBiomech.com

Design and validation of a testing system to assess torsional cancellous bone failure in conjunction with time-lapsed micro-computed tomographic imaging

Ara Nazarian [a,c], Michael Bauernschmitt [c,1], Christian Eberle [c,1], Diego Meier [a,c], Ralph Müller [d], Brian D. Snyder [a,b,*]

[a] Orthopedic Biomechanics Laboratory (OBL), Beth Israel Deaconess Medical Center and Harvard Medical School, 330 Brookline Avenue, RN115, Boston, MA 02215, USA
[b] Department of Orthopaedic Surgery, Children's Hospital, Harvard Medical School, Boston, MA 02115, USA
[c] Institute for Biomedical Engineering, University and ETH Zürich, 8044 Zürich, Switzerland
[d] Institute for Biomechanics, ETH Zurich, 8092 Zurich, Switzerland

ARTICLE INFO

Article history:
Accepted 23 September 2008

Keywords:
Cancellous bone
Torsion testing
Shear properties
Micro-computed tomography

ABSTRACT

When compressed axially, cancellous bone often fails at an oblique angle along well-defined bands, highlighting the importance of cancellous bone shear properties. Torsion testing to determine shear properties of cancellous bone has often been conducted under conditions appropriate only for axis-symmetric specimens comprised of homogeneous and isotropic materials. However, most cancellous bone specimens do not meet these stringent test conditions. Therefore, the *aim* of this study was to design and validate a uniaxial, incremental torsional testing system for non-homogeneous orthotropic or non-axis-symmetric specimens.

Precision and accuracy of the newly designed torsion system was validated by using Plexiglas rods and beams, where obtained material properties were compared to those supplied by the manufacturer. Additionally, the incremental step-wise application of angular displacement and simultaneous time-lapsed μCT imaging capability of the system was validated using whale cancellous bone specimens, with step-wise application of angular displacement yielding similar torsional mechanical properties to continuous application of angular displacement in a conventional torsion study.

In conclusion, a novel torsion testing system for non-homogeneous, orthotropic materials using the incremental step-wise application of torsion and simultaneous time-lapsed μCT imaging was designed and validated.

1. Introduction

Better understanding of microstructure–function relationships in cancellous bone can provide insight in the determination of non-traumatic fracture risk associated with metabolic bone diseases and help to optimize pharmacological interventions by blocking bone resorption and/or promoting bone formation. Relationships between cancellous bone material properties and trabecular microstructure have been established for normal and pathologic, human and animal bone specimens in tension or compression (Kleerekoper et al., 1985; Parfitt et al., 1985; Rao et al., 1985; Poodenphant et al., 1987; Chung et al., 1993; Recker, 1993; Ulrich et al., 1997; Thomsen et al., 1998; Niebur et al., 2000; Ikeda et al., 2001; Turner et al., 2001; Wachter et al., 2001; Ding et al., 2002). Time-lapsed micro-computed tomographic imaging and compression of cancellous bone has been used to evaluate the modes of trabecular failure for mostly plate-like whale trabecular bone (Nazarian and Müller, 2004), and mostly rod-like human trabecular bones (Nazarian and Müller, 2004; Nazarian et al., 2005). When compressed axially, cancellous bone specimens often fail along well-defined bands at an oblique angle to the longitudinal axis implying that shear may contribute to the mechanism of failure (Silva and Gibson, 1997; Müller et al., 1998). While shear properties of cancellous bone have been reported previously (Sammarco et al., 1971; Halawa et al., 1978; Stone et al., 1983; Fyhrie and Schaffler, 1994; Mitton et al., 1997), many of the torsion tests performed to determine these properties were conducted under conditions appropriate only for

* Corresponding author at: Orthopedic Biomechanics Laboratory (OBL), Beth Israel Deaconess Medical Center and Harvard Medical School, 330 Brookline Avenue, RN115, Boston, MA 02215, USA. Tel.: +1 617 667 2940; fax: +1 617 667 7175.
E-mail address: bsnyder@bidmc.harvard.edu (B.D. Snyder).
[1] Authors two and three have contributed equally to this work.

0021-9290/$ - see front matter © 2008 Elsevier Ltd. All rights reserved.
doi:10.1016/j.jbiomech.2008.09.014

axis-symmetric specimens comprised of homogeneous and isotropic materials (Ford and Keaveny, 1996; Bruyere Garnier et al., 1999). Similar tests have also been performed to assess torsional properties of rodent long bones (Brodt et al., 1999; Silva and Ulrich, 2000; Kasra and Grynpas, 2008). However, most cancellous bone and rodent long bones do not meet these conditions; since trabecular microstructure is often heterogeneous, anisotropic and the predominant trabecular orientation is not aligned along the centroidal axis of the specimen. If a non-axis-symmetric, orthotropic bone specimen is subjected to torsion, it will warp and bend out of plane due to coupling between the mutually orthogonal normal and shear strains induced by the applied torque (Hermann, 1965) (Fig. 1). If both ends of a non-axis-symmetric specimen are coaxially fixed to the load frame during torsion testing, the free movement of the neutral axis of the specimen will be restricted. When torque is applied along the centroidal axis of the specimen, the loading profile is contaminated by additional (and unaccounted) bending moments that restrict the specimen's out of plane deformation. We have performed twisting and pure torsion tests on similar specimens and have found an average underestimation of 19% for shear modulus and an average overestimation of 12% for ultimate shear strength in the twisting cases. Therefore, the *aim* of this study is to design and validate a uniaxial torsional testing system for non-homogeneous orthotropic or non-axis-symmetric specimens that accommodates out of plane warping and bending, while providing concurrent visualization of specimen deformation using sequential micro-computed tomography (μCT) and incremental application of torque.

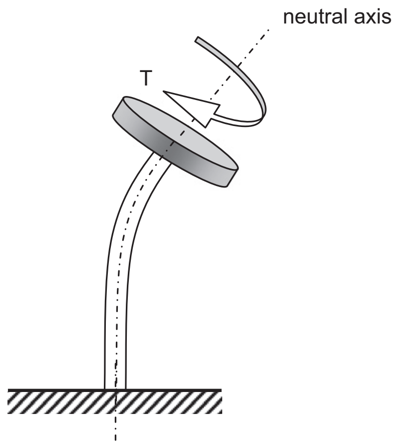

Fig. 1. A schematic illustration highlighting out of plane warping of a non-axis-symmetric, orthotropic specimen subjected to torsion.

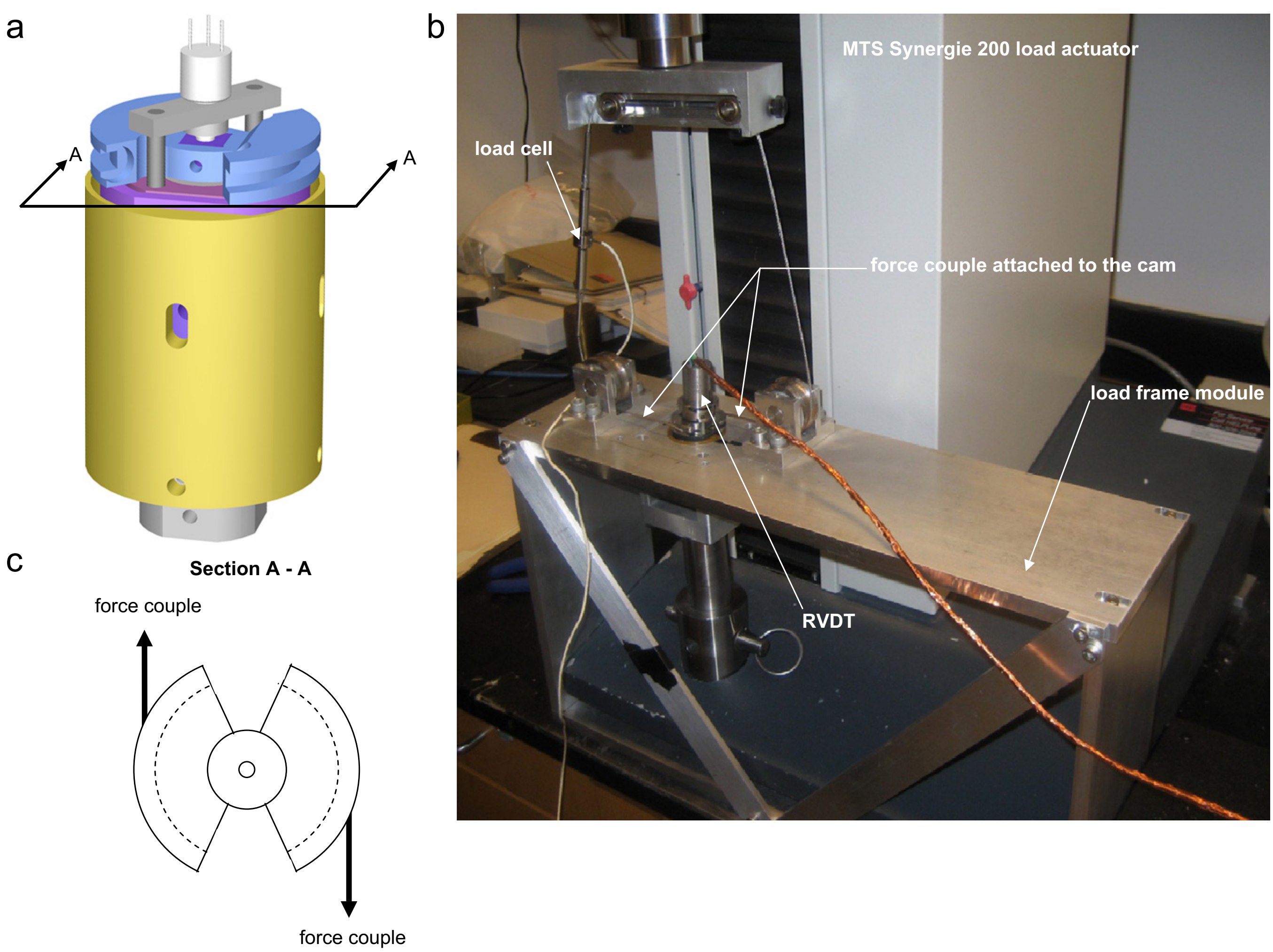

Fig. 2. (a) Schematic presentation of the specimen module; the specimen is placed within the green area, and the coupling cables are attached to the blue color pulley. Section A–A demonstrated the manner in which the force couple is applied via a pair of cables: (b) an image of the load frame module and (c) a representation of the force couple system.

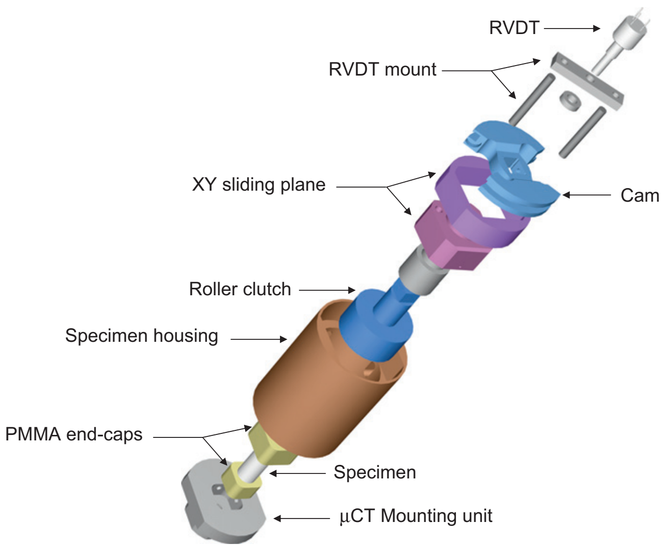

Fig. 3. The assembly drawing of the torsion testing system highlighting the comprising components and their coupling with the specimen onboard.

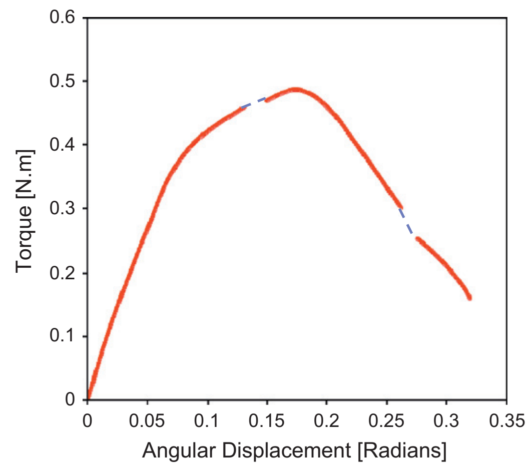

Fig. 4. A sample data reconstruction to create a continuous angular displacement–torque diagram from a set of discrete curves.

2. Methods

2.1. System design

The system is comprised of a specimen and a load frame module (Fig. 2a and b). The specimen module consists of a μCT mounting unit, a specimen housing, a cam to which cables forming the force couple are connected to (Fig. 2c), a rotary variable differential transformer (RVDT) to measure the applied angular displacement (RSYN-8-30, range $\pm 30^{\circ}$, sensitivity $0.013 \pm 5\%$ V/V/Deg, linearity $\pm 0.5\%$ full scale output, Lucas Schaevitz, Hampton, VA, USA), a miniature universal joint, a sliding table (comprised of two PTFE-coated collars) to accommodate out of plane warping and bending of non-axis-symmetric specimens and a roller clutch (FCL 10K, MTO & Co., Bad Ragaz, Switzerland) that maintains the angular displacement applied to the specimen for the duration of μCT imaging (Fig. 3). The load frame module provides an adjustable interface between the specimen module and the load actuator (MTS Synergie 200, Eden Prairie, MN, USA). To measure the applied torque, a load cell (Burster 8417 Subminiature Tension/Compression load cell, range 1000 N, accuracy $< \pm 0.5\%$ full scale output, Neuhausen, Switzerland) is mounted in line with the cable used to generate the force couple (Fig. 2a). The load actuator (MTS Synergie 200) and the transducers are connected to a PCI-MIO-16E4 data acquisition card (National Instruments, Austin, TX, USA) controlled using a LabView program (National Instruments, Austin, TX, USA). The National Instruments card communicate with the load actuator via a serial port connection to give operational commands and records the signals received from the transducers as a TXT file.

2.2. Specimen preparation

Plexiglas (polymethylmethacrylate), an engineering material with known material properties similar to that of cortical bone was used to validate the torsion system (Turner and Burr, 1993; Cowin, 2001). The system was validated with cylindrical ($\varnothing$: 4.0 mm, H: 36.0 mm, $n = 5$) Plexiglas rods and rectangular (W: 4.0 mm, D: 4.0 mm, H: 36.0 mm, $n = 5$) Plexiglas beams (Mc Master Carr, New Brunswick, NJ, USA). Additionally, similar rectangular Plexiglas beams ($n = 5$) were used to test the repeatability of the testing system.

Cancellous bone specimens of similar density and trabecular microstructure were cored from a vertebral body harvested from a beached Bowhead whale (*Balaena mysticetus*) in the north eastern United States along the cephalo-caudal axis as described previously (Nazarian and Müller, 2004). Five pairs of cored trabecular bone specimens matched by bone mass and volume fraction were randomly assigned to undergo torsional testing either at a continuous ramp (CONT) or incremental step-wise (SW) fashion.

2.3. μCT imaging

Images of the cancellous bone specimens were acquired using a μCT 40 (Scanco Medical AG, Bassersdorf, Switzerland) at 70 kVp energy, 114 μA current, 250 ms integration time, and 30 μm isotropic voxel size (Ruegsegger et al., 1996). A three-dimensional Gaussian filter ($\sigma = 0.8$) with limited finite filter support (support = 1) was used to suppress the noise in the volumes.

2.4. Mechanical testing

The ends of all specimens were embedded in a PMMA end-cap to facilitate gripping of the specimen and minimize crushing artifact. Continuous or incremental SW angular displacement in clockwise direction was applied to specimens based on their grouping. In order to address stress relaxation concerns with the discrete SW testing modality, the results of the SW testing mode were compared to: (a) results obtained from a conventional continuous torsion test (gold standard for torsion testing) using the same system and identical testing conditions, and (b) the mechanical properties of Plexiglas supplied by the manufacturer. Cylindrical rods and rectangular beams were used to validate Plexiglas mechanical properties to account for our of plane warping.

The SW incremental testing protocol consisted of μCT imaging of the specimen at zero angular displacement. This step was followed by the application of angular displacement of 0.13 (7.5°), 0.26 (15.0°), 0.35 (20.0°) and 0.44 rad (25.0°) with μCT imaging at the conclusion of each angular displacement step. Following the application of each step, the specimen was allowed to relax for 20 min prior to its transfer to the μCT for imaging (imaging duration ~60 min). The 20 min window was chosen based on experiments performed to establish an appropriate time interval for specimens to reach a plateau for stress relaxation. The SW angular displacement–torque diagrams consisted of three discrete sections between the four strain steps of 0, 0.13, 0.26, 0.35, and 0.44 rad angular displacements. In order to address these drops and obtain a continuous angular displacement–torque diagram, the end point of discrete section was connected to the beginning point of the next discrete section via a straight line (dashed lines in Fig. 4), based on the assumption that the results obtained from the reconstructed SW tests would be compatible with those obtained from continuous tests. This measure is an arbitrary method of generating continuous diagrams from the SW data and has been used successfully in SW compression (Nazarian and Müller, 2004; Nazarian et al., 2005). We used the validation results to address whether the addition of these lines would give rise to a method (SW) capable of accurately reflecting the mechanical properties of the samples established by conventional continuous tests.

The continuous testing protocol consisted of application of angular displacement of 0.44 rad (25.0°) to the specimens. Both CONT and SW tests were performed at an angular displacement rate of 0.083 rad s^{-1}. Ultimate torque (T_{ULT}, N m—maximum torque reached on the torque–angular displacement diagram), torsional stiffness (K_{TOR}, N m rad^{-1}), ultimate shear strength (τ_{ULT}, MPa—maximum strength reached on the shear strength–strain diagram) and strain (γ_{ULT}) and shear modulus (G, MPa) were measured for both CONT and SW specimens. The specimens remained hydrated during testing, where wet gauze was wrapped around them to maintain hydration during mechanical testing. This was verified upon retrieval of wet specimens at the end of each test.

Calculations of the shear strength and shear modulus of elasticity for all cases in the study are detailed in the Appendix A.

2.5. Statistical analysis

Analysis of variance (ANOVA) was performed to compare continuous and SW torsional properties with testing modality as the fixed factor and mechanical properties as dependent variables. The SPSS statistical package (version 15.0, Chicago, Illinois, USA) was used for data analysis. All reported p-values are two-tailed with $p < 0.05$ considered statistically significant.

Table 1
Mechanical properties (mean and standard deviation in parentheses) of Plexiglas cylindrical rods and rectangular beams undergoing conventional continuous torsion in comparison to those obtained from the manufacturer

	Ultimate shear strength (MPa)	Shear modulus (MPa)	Modulus of elasticity (MPa)
Average provided by manufacturer	60.0	1100.0	3000.0
CONT cylindrical rods—average (Standard deviation)	58.5 (1.87)	1094.2 (26.27)	2969.6 (79.28)
Coefficient of variation (%)	3.2	2.4	2.7
Percent difference (versus manufacturer)	−2.5	−0.5	−1.0
CONT rectangular beams—average (Standard deviation)	59.3 (2.11)	1092.1 (36.42)	2963.9 (93.78)
Coefficient of variation (%)	3.5	3.3	3.1
Percent difference (versus manufacturer)	−1.1	−0.7	−1.2

3. Results

Material properties of circular Plexiglas rods and rectangular Plexiglas beams obtained from the manufacturer and from conventional continuous torsion testing performed in this study are shown in Table 1. The measured elasticity and shear moduli values are within 1.2% of the manufacturer's specifications, while the measured shear strength is within 2.7% of the shear strength specified by the manufacturer. The torque–angular displacement curves of two representative circular Plexiglas rod and rectangular Plexiglas beam undergoing torsion testing demonstrate classic brittle failure characteristics (Fig. 5a and b). Less than one percent intra-specimen variation was observed in the torque results, based on the repetitive non-failure precision tests performed on the same specimens.

The mass and BV/TV of the specimens randomly assigned to the CONT and SW cancellous bone groups were almost identical with inter group differences of 1.4% and 2.4%, respectively (Table 2). The torsional mechanical properties obtained by the incremental application of SW torque were not significantly different from those obtained via the application of continuous angular displacement (Table 2). Visual observation of the incremental μCT images reveal an initial pattern of trabecular bending along shear lines followed by the disconnection of trabecular elements from the specimen under increasing angular displacement, resulting in burst failure and separation of a portion of the cancellous bone in the region of failure (Fig. 6).

In order to compare the differences between twisting and pure torsion tests, three pairs of similar specimens (matched mass and bone volume fraction values) were subjected to twisting and pure torsion testing. The results showed an average underestimation of 19% for shear modulus (twisting: 593.86 ± 75.21 MPa, torsion: 726.24 ± 84.32 MPa) and an average overestimation of 12% for ultimate shear strength (twisting: 16.68 ± 5.47 MPa, torsion: 14.56 ± 5.06 MPa) in the twisting cases.

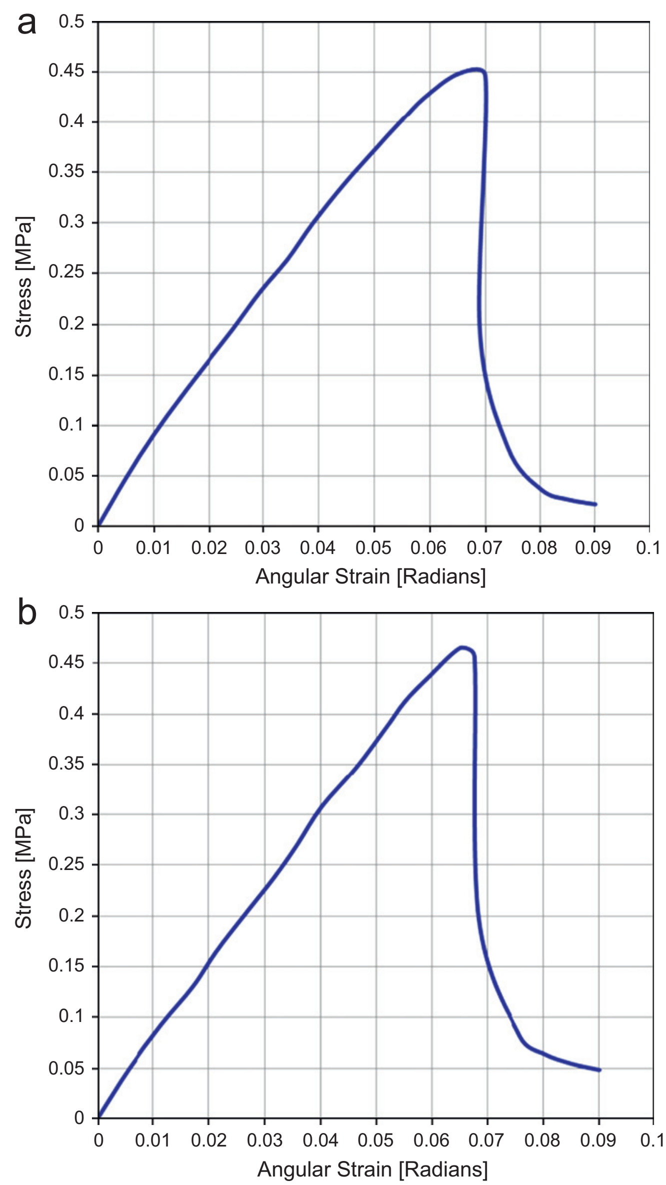

Fig. 5. Angular strain versus stress diagram of a representative (a) circular Plexiglas rod and a (b) rectangular Plexiglas beam.

4. Discussion

The Plexiglas rod and beam mechanical properties obtained from the new torsion testing system were almost identical to those supplied by the manufacturer, validating the accuracy of the system. Additionally, the small variation (coefficient of variation $<3.5\%$ for all measures) reported in the mechanical properties of 5 similar Plexiglas rods undergoing identical torsional testing, validated the precision of the testing system. Supplementary precision validation revealed $<1\%$ intra-specimen variation from repetitive testing of identical rectangular Plexiglas beams.

Additionally, the incremental SW application of angular displacement and simultaneous time-lapsed μCT imaging capability of the system was validated using whale cancellous bone specimens, with SW application of angular displacement yielding similar torsional mechanical properties to continuous application of angular displacement in a conventional torsion study ($p > 0.4$ for all cases).

In conclusion, a novel torsion testing system for non-homogeneous, orthotropic materials using the incremental SW

Table 2
Average specimen and mechanical properties (mean and standard deviation in parentheses) for whale cancellous bone specimens undergoing either conventional continuous or SW torsion testing

	Mass (g)	BV/TV (mm^3/ mm^3)	Max torque (N m)	Torsional stiffness (N m/rad)	Ultimate shear strength (MPa)	Ultimate shear strain (%)	Shear modulus (MPa)
Average continuous (Standard deviation)	2.14 (0.14)	0.41 (0.07)	4.51 E-4 (0.6 E-4)	4.21 E-4 (0.10 E-4)	14.81 (4.13)	0.06 (0.02)	732.21 (79.08)
Average SW test (Standard deviation)	2.17 (0.17)	0.42 (0.07)	4.84 E-4 (0.4 E-4)	4.61 E-4 (0.12 E-4)	15.34 (3.62)	0.08 (0.03)	779.13 (82.72)
Percent difference (%)	1.4	2.4	−7.3	−9.2	−3.5	30.3	−6.4
p-Value	0.6	0.9	0.7	0.6	0.8	0.5	0.5

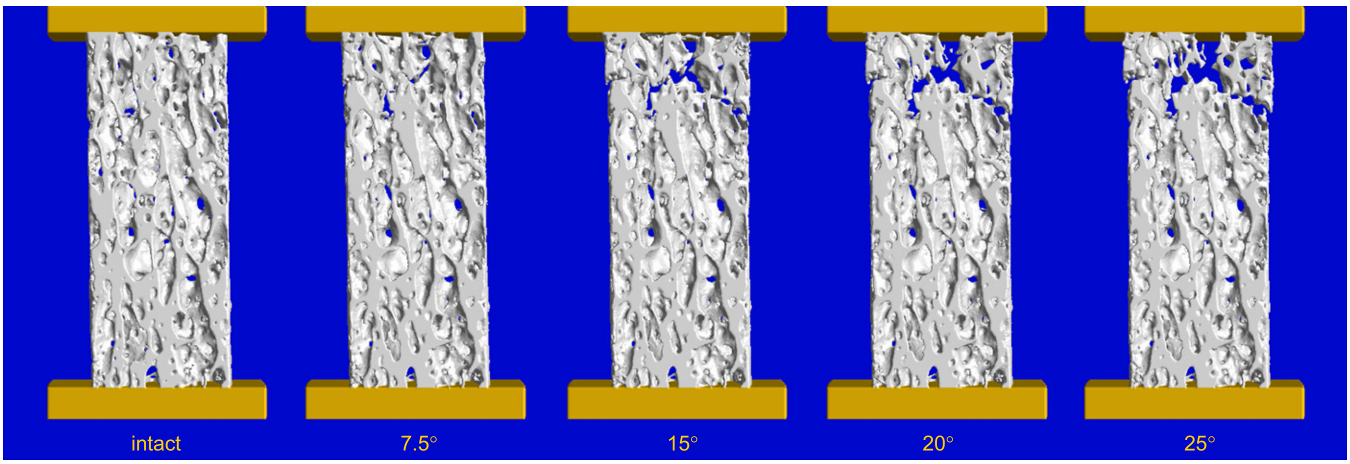

Fig. 6. Torsion steps of 0 (intact), 7.5°, 15°, 20°, and 25° angular displacement on a representative specimen. The figure represents a coronal view of a representative specimen displaying the failure patters experienced by the trabecular microstructure. The red box super-imposed on the 25° angular displacement image highlights the shear failure plane observed in the specimen.

application of torsion and simultaneous time-lapsed μCT imaging was designed and validated. This approach enables one to perform proper continuous torsion testing and/or incremental SW testing in order to obtain both mechanical and visual insight in the failure modes of structures of interest.

Conflict of interest statement

None.

Acknowledgments

The authors would like to acknowledge the ETH Electrical Engineering Department's machining facility and Boston University Physics Department's Scientific Instrument Facility for their help with the manufacturing and subsequent modifications of the design. The authors would like to acknowledge the insight comments made by the reviewers which have been directly incorporated into the manuscript.

Appendix A. Supporting Information

Supplementary data associated with this article can be found in the online version at doi:10.1016/j.jbiomech.2008.09.014.

References

Brodt, M.D., Ellis, C.B., Silva, M.J., 1999. Growing C57Bl/6 mice increase whole bone mechanical properties by increasing geometric and material properties. Journal of Bone and Mineral Research 14, 2159–2166.

Bruyere Garnier, K., Dumas, R., Rumelhart, C., Arlot, M.E., 1999. Mechanical characterization in shear of human femoral cancellous bone: torsion and shear tests. Medical Engineering and Physics 21, 641–649.

Chung, H., Wehrli, F.W., Williams, J.L., Kugelmass, S.D., 1993. Relationship between NMR transverse relaxation, trabecular bone architecture, and strength. Proceedings of the National Academy of Science USA 90, 10250–10254.

Cowin, S.C. (Ed.), 2001. Bone Mechanics Handbook. CRC Press, Boca Raton.

Ding, M., Odgaard, A., Linde, F., Hvid, I., 2002. Age-related variations in the microstructure of human tibial cancellous bone. Journal of Orthopaedic Research 20, 615–621.

Ford, C.M., Keaveny, T.M., 1996. The dependence of shear failure properties of trabecular bone on apparent density and trabecular orientation. Journal of Biomechanics 29, 1309–1317.

Fyhrie, D.P., Schaffler, M.B., 1994. Failure mechanisms in human vertebral cancellous bone. Bone 15, 105–109.

Halawa, M., Lee, A.J., Ling, R.S., Vangala, S.S., 1978. The shear strength of trabecular bone from the femur, and some factors affecting the shear strength of the cement–bone interface. Archives of Orthopaedic and Trauma Surgery 92, 19–30.

Hermann, L.R., 1965. Elastic torsional analysis of irregular shapes. Proceedings of the American Society of Civil Engineers 91, 11–19.

Ikeda, S., Tsurukami, H., Ito, M., Sakai, A., Sakata, T., Nishida, S., Takeda, S., Shiraishi, A., Nakamura, T., 2001. Effect of trabecular bone contour on ultimate strength of lumbar vertebra after bilateral ovariectomy in rats. Bone 28, 625–633.

Kasra, M., Grynpas, M.D., 2008. On shear properties of trabecular bone under torsional loading: effects of bone marrow and strain rate. Journal of Biomechanics 40 (13), 2793–2798.

Kleerekoper, M., Villanueva, A.R., Stanciu, J., Rao, D.S., Parfitt, A.M., 1985. The role of three-dimensional trabecular microstructure in the pathogenesis of vertebral compression fractures. Calcified Tissue International 37, 594–597.

Mitton, D., Rumelhart, C., Hans, D., Meunier, P.J., 1997. The effects of density and test conditions on measured compression and shear strength of cancellous bone from the lumbar vertebrae of ewes. Medical Engineering and Physics 19, 464–474.

Müller, R., Gerber, S.C., Hayes, W.C., 1998. Micro-compression: a novel technique for the nondestructive assessment of local bone failure. Technology and Health Care 6, 433–444.

Nazarian, A., Müller, R., 2004. Time-lapsed microstructural imaging of bone failure behavior. Journal of Biomechanics 37, 55–65.

Nazarian, A., Stauber, M., Müller, R., 2005. Design and implementation of a novel mechanical testing system for cellular solids. Journal of Biomedical Materials Research Part B: Applied Biomaterials 73, 400–411.

Niebur, G.L., Feldstein, M.J., Yuen, J.C., Chen, T.J., Keaveny, T.M., 2000. High-resolution finite element models with tissue strength asymmetry accurately predict failure of trabecular bone. Journal of Biomechanics 33, 1575–1583.

Parfitt, A.M., Rao, D.S., Stanciu, J., Villanueva, A.R., Kleerekoper, M., Frame, B., 1985. Irreversible bone loss in osteomalacia. Comparison of radial photon absorptiometry with iliac bone histomorphometry during treatment. Journal of Clinical Investigation 76, 2403–2412.

Poodenphant, J., Nielsen, V.A., Riis, B.J., Gotfredsen, A., Christiansen, C., 1987. Bone mass, bone structure and vertebral fractures in osteoporotic patients. Bone 8, 127–130.

Rao, D.S., Parfitt, A.M., Kleerekoper, M., Pumo, B.S., Frame, B., 1985. Dissociation between the effects of endogenous parathyroid hormone on adenosine 3′,5′-monophosphate generation and phosphate reabsorption in hypocalcemia due to vitamin D depletion: an acquired disorder resembling pseudohypoparathyroidism type II. Journal of Clinical Endocrinology and Metabolism 61, 285–290.

Recker, R.R., 1993. Architecture and vertebral fracture. Calcified Tissue International 53 (Suppl 1), S139–142.

Ruegsegger, P., Koller, B., Muller, R., 1996. A microtomographic system for the nondestructive evaluation of bone architecture. Calcified Tissue International 58, 24–29.

Sammarco, G.J., Burstein, A.H., Davis, W.L., Frankel, V.H., 1971. The biomechanics of torsional fractures: the effect of loading on ultimate properties. Journal of Biomechanics 4, 113–117.

Silva, M.J., Gibson, L.J., 1997. Modeling the mechanical behavior of vertebral trabecular bone: effects of age-related changes in microstructure. Bone 21, 191–199.

Silva, M.J., Ulrich, S.R., 2000. In vitro sodium fluoride exposure decreases torsional and bending strength and increases ductility of mouse femora. Journal of Biomechanics 33, 231–234.

Stone, J.L., Beaupre, G.S., Hayes, W.C., 1983. Multiaxial strength characteristics of trabecular bone. Journal of Biomechanics 16, 743–752.

Thomsen, J.S., Ebbesen, E.N., Mosekilde, L., 1998. Relationships between static histomorphometry and bone strength measurements in human iliac crest bone biopsies. Bone 22, 153–163.

Turner, C.H., Burr, D.B., 1993. Basic biomechanical measurements of bone: a tutorial. Bone 14, 595–608.

Turner, C.H., Hsieh, Y.F., Müller, R., Bouxsein, M.L., Rosen, C.J., McCrann, M.E., Donahue, L.R., Beamer, W.G., 2001. Variation in bone biomechanical properties, microstructure, and density in BXH recombinant inbred mice. Journal of Bone and Mineral Research 16, 206–213.

Ulrich, D., Hildebrand, T., Van Rietbergen, B., Muller, R., Ruegsegger, P., 1997. The quality of trabecular bone evaluated with micro-computed tomography, FEA and mechanical testing. Study of Health Technology Information 40, 97–112.

Wachter, N.J., Augat, P., Hoellen, I.P., Krischak, G.D., Sarkar, M.R., Mentzel, M., Kinzl, L., Claes, L., 2001. Predictive value of Singh index and bone mineral density measured by quantitative computed tomography in determining the local cancellous bone quality of the proximal femur. Clinical Biomechanics 16, 257–262 (Bristol, Avon).